Molecular insights into the effect of anionic-nonionic and cationic surfactant mixtures on interfacial properties of oil-water interface

Wenning Zhou[a,b,*], Long Jiang[a], Xunliang Liu[a,b], Yang Hu[c], Yuying Yan[d]

[a]School of Energy and Environmental Engineering, University of Science and Technology Beijing, Beijing 100083, China

[b]Beijing Key Laboratory of Energy Conservation and Emission Reduction for Metallurgical Industry, Beijing 100083, China

[c]School of Civil and Resources Engineering, University of Science and Technology Beijing, Beijing 100083, China

[d]Fluids & Thermal Engineering Research Group, Faculty of Engineering, University of Nottingham, Nottingham NG7 2RD, UK

[*]Corresponding author:

Dr. Zhou, Email: wenningzhou@ustb.edu.cn

Abstract

The influence of surfactants is of great importance to the interfacial properties, which is related by the characteristics of molecular arrays at the interface of multicomponent and multiphase systems. Comparing with single type of surfactant, the mixtures of surfactants usually provide superior performances in improving interfacial properties of the oil-water interface in the application of enhanced oil recovery. In this study, molecular dynamics simulations were employed to explore the mechanisms and interfacial behaviors at the microscopic level of pure and binary mixture of anionic-nonionic surfactant alcohol ether sulfates (AES) and cationic surfactant dodecyltrimethylammonium chloride (DTAC) at oil-water interface. The results show that the sulfate groups of AES molecules could attract DTAC molecules in the mixed surfactants, thereby reducing the repulsion between the molecules. DTAC molecules present excellent molecular interfacial behaviors, which could improve the arrangement of AES molecules through the interactions between head groups. In addition, it is found that the number of ethylene oxide (EO) group of AES molecules has a great influence on the behaviors of interface. An increase of EO group number could cause AES molecules to exhibit varying degrees of bending. By controlling the proper number of EO group, the aggregation of surfactants could be avoided and satisfactory interfacial properties will be achieved. Moreover, it is observed that the positive charge of DTAC molecule shows a strong repulsion to salt ions, for example Ca^{2+} ions, thus enhancing the overall salt resistance of mixed surfactants. The molecular-level insights gained in this work could provide useful guidance for designing the surfactant formulations for tertiary/enhanced oil recovery in low-permeability unconventional reservoirs.

Keywords: interfacial behavior; mixed surfactants; molecular dynamics simulation; anionic-nonionic surfactant; cationic surfactant.

1. Introduction

Oil resources play a crucial role in the development of society. In order to meet the increasing demand for oil resources along with the continuous and rapid growth of economy, the enhancement of oil recovery is of great importance. In the early stage of reservoir formation, a large number of crude oil polar molecules blocked the pore throat of the reservoir, which has greatly increased the difficulty of oil recovery. After primary and secondary oil recovery, 60–70% of the residual oil resources still remain under the ground and need to be further exploited [1]. Therefore, the tertiary or enhanced oil recovery (EOR) technologies, including thermal recovery, steam injection, chemical flooding, and microbial flooding, have been proposed. Chemical flooding, which involves the mobilization and displacement of trapped oil by injecting chemicals (e.g., polymer, alkaline, surfactant, etc.), has shown obvious advantages among various EOR technologies [2-4].

Surfactants are widely utilized in chemical oil recovery enhancement applications due to their hydrophilic-lipophilic abilities, which could be used in adjusting interfacial behaviors of oil-water interface [5-9]. In realistic EOR project, considering the complicated conditions of the oilfield, more than one type of surfactant, mixed surfactants, nanoparticles, and other additives might be introduced to obtain the optimal interfacial performances [10-12]. So far extensive research work has been conducted in this field. Saha et al. [13] used an extracted natural surfactant (Reetha), a polymer, and silica nanoparticles to improve the viscosity and stability of the emulsion. They claimed that the high-viscosity emulsion could block water channeling, thereby diverting the oil displacement fluid to oil-rich zone as well as improving the sweep efficiency. Vatanparast et al. [14] experimentally examined the adsorption properties of nonionic surfactant at water-heptane interface with the presence of silica nanoparticle. They argued that the non-electrostatic interactions could exhibit different impacts on the interfacial behaviors depending on the type of surfactant. Adkins et al. [15] reported a new type of anionic surfactant alkyl ethoxy sulfate, which could remain stable for a long time at temperatures up to 83°C even

with the presence of divalent ions. Torres and his co-workers [16] found the natural surfactant rhamnolipid produced by *Pseudomonas* and guar gum exhibits good abilities to improve surface tension, foaming capability as well as resistance to salinity and high temperatures.

In addition to experimental studies, molecular simulation has recently become a powerful tool to explore the underlying mechanisms of a wide variety of complex phenomena at the microscopic level [17-23]. In particular, molecular dynamics (MD) simulation has been widely adopted to examine the microscopic mechanism of the interfacial characteristics at oil-water interface [24-28]. Shi et al. [29] applied molecular dynamics to study the interfacial behaviors of anionic, nonionic, zwitterionic, and gemini surfactants. By calculating the interfacial thickness, radial distribution function, and interfacial formation energy, they found that gemini surfactant is the most advantageous in reducing interfacial tension among them. Ivanova et al. [30] discussed the influences of temperature on the performances of surfactant. The results showed that with the increasing temperature, the hydrogen bondings between head groups of surfactants and water molecules decrease, and thus the solubility of surfactant molecule in water also declines. Yan et al. [31] investigated the oil displacement effect of sulfonate and sulfate with the presence of Na^{+}, Ca^{2+}, and Mg^{2+}. Their results have shown that sulfonate is more stable in brine than sulfate and also has higher oil recovery efficiency. From the abovementioned research, it can be concluded that different types of surfactant would exhibit different influences on interfacial properties as well as salt- and temperature-resistance.

In order to adapt to the actual complex conditions of oil reservoirs, mixed surfactants have been recently considered in field operations due to their superior stability and physicochemical properties, e.g., mixed cationic/anionic surfactants [32, 33], mixed ionic/nonionic surfactants [10, 34-36], zwitterionic surfactants [37-39], and gemini surfactants [40, 41]. Jia et al. [32] examined the impacts of mixed cationic/anionic surfactants at oil-water interface. They found that the mixed systems have great improvements in reducing interfacial tension and stabilizing oil-in-water emulsion compared with pure surfactant. However, it is difficult to implement mixed cationic

and anionic surfactants in particle EOR application because of the low solubility, precipitation, and strict proportions of the combined systems. Due to the unique structures of zwitterionic and gemini surfactants, they exhibit excellent performances of high solubility, remarkable interfacial behaviors, good foam stability as well as resistance to high salinity and temperature [42, 43]. But the high production costs of zwitterionic and gemini surfactants make them difficult to be widely used in oilfield production. Thus, the mixings of zwitterionic/gemini surfactants and low-cost ionic surfactants have been recently focused by many researchers. Cai et al. [44] conducted a comparative study of binary zwitterionic betaine-type and anionic surfactant mixture chosen from two zwitterionic surfactants and three anionic surfactants. Their results indicated that the appropriate hydrophilic-lipophilic balance and suitable structure are essential for anionic surfactant to achieve matched lipophilic and hydrophilic group when cooperating with of betaine. Feng and his co-workers [45] experimentally investigated a combined cationic and anionic-nonionic gemini surfactant system under realistic reservoir conditions. They claimed that mixed surfactants show notable interactive properties and could be considered to be an ideal candidate for EOR. Although a few studies have been carried out for investigating the behaviors of gemini surfactants and their mixed system with other surfactants, most of them focused on the macroscopic-level properties [46-49]. An in-depth understanding of the underlying structure–function relationship of the adsorbed surfactants on the interface is necessary.

In this study, molecular dynamic simulation was applied to explore the microscopic insights of the mixed cationic surfactant dodecyltrimethylammonium chloride (DTAC) and anionic-nonionic gemini surfactant AES ($C_{12}H_{25}(OCH_2CH_2)_nSO_4Na$) containing n-ethylene oxide (EO) groups. The proposed model was firstly validated by comparing with experimental data. Then the effects of pure and mixed surfactants on the interfacial behaviors of oil-water interface were investigated. The influences of mixing ratio and EO group number of mixed system on interfacial performances were discussed in detail. Finally, the salt resistances of pure and mixed surfactants were examined.

2. Models and methods

2.1 Force field

In this work, all molecular dynamics simulations were performed in the Forcite and Amorphous modules of Materials Studio package (version 2017). Water molecules were described by the SPC/E model. The charges and potential functions of the alkane and surfactants were determined by the COMPASS force field [50]. The potential energy is written as:

$$E_{\text{total}} = E_{\text{bonds}} + E_{\text{angles}} + E_{\text{dihedrals}} + E_{\text{out-of-plane}} + E_{\text{cross}} + E_{\text{vdW}} + E_{\text{elec}} \quad (1)$$

where the first five items on the right side are the valence terms including diagonal and off-diagonal terms, namely, the internal coordinates of bond, angle, torsion angle, out-of-plane angle, and the cross terms. The last two terms denote non-bond interactions. Specifically, the van der Waals interaction between molecules was described by L-J function with the cutoff radius of 0.95 nm. The Ewald method was adopted to deal with the long-range electrostatic interaction, i.e., the Coulomb potentials. The calculation formulas can be expressed as:

$$E_{\text{vdW}} = \sum \varepsilon_{ij} \left[2 \left(\frac{r_{ij}^0}{r_{ij}} \right)^9 - 3 \left(\frac{r_{ij}^0}{r_{ij}} \right)^6 \right] \quad (2)$$

$$E_{elec} = \sum \frac{q_i q_j}{\varepsilon_0 r_{ij}} \quad (3)$$

where r_{ij} denotes the distance between atoms i and j. ε_0 is the relative dielectric constant. q_i and q_j represent the charges of atoms i and j, respectively. r_{ij}^0 is equilibrium distance for the i, j atom pair and ε_{ij} is the L-J well depth, which can be determined by the 6th-power rule [50].

2.2 Models and simulation details

To study the synergistic mechanism of mixed surfactants, a water layer containing 3500 water molecules was firstly established. Then a total of 60 anionic-nonionic surfactant AES molecules and cationic surfactant DTAC molecules were placed on the both ends of water layer to form two surfactant layers for faster relaxation. Finally,

350 n-decane molecules were placed at the each end of surfactants. The cross-sectional area of the system was 5 × 5 nm^2 and the length of simulation box was 22 nm. According to different ratios of surfactants, seven mixed systems were established, as shown in Table 1. The initial model of system S60, taking EO number n = 3 as an example, is shown in Fig. 1. To examine the salt resistance of the system, 20 Ca^{2+} and 40 Cl^- ions were introduced into the water phase.

Table 1. Different ratios of mixed surfactants and the number of molecules in each surfactant system.

System	$C_{12}EO_nS$/DTAC	$C_{12}EO_nS$	DTAC
S60	10:0	60	0
S48D12	8:2	48	12
S36D24	6:4	36	24
S30D30	5:5	30	30
S24D36	4:6	24	36
S12D48	2:8	12	48
D60	0:10	0	60

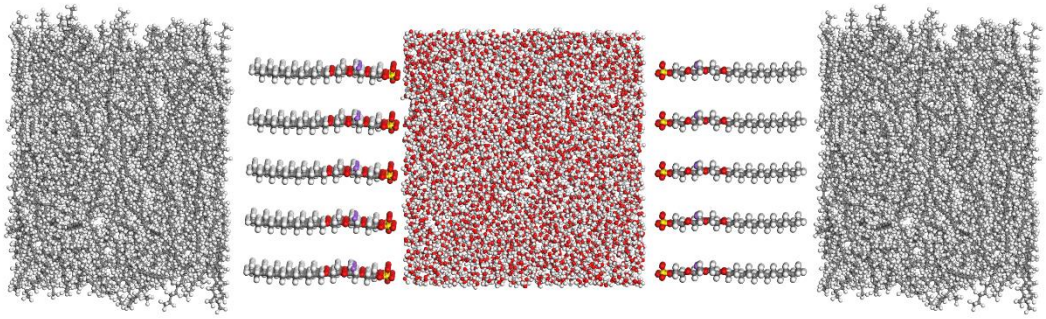

Fig. 1. The initial model of the system S60.

In addition to studying different ratio of the mixed system, the influences of nonionic fragments EO group number of AES molecules on interfacial behaviors were discussed. The structures of AES molecules with different numbers of EO group are shown in Fig. 2.

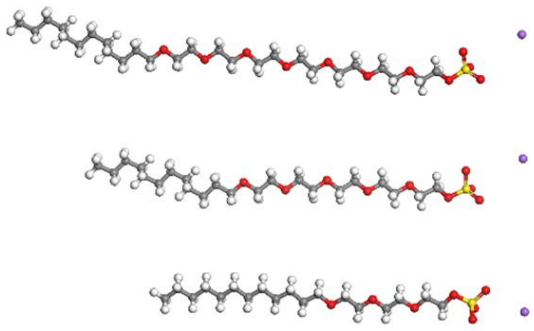

Fig. 2. The structure of surfactants AES $C_{12}EO_nS$ with different EO group numbers (from top to bottom, the numbers of EO group are equal to 7, 5, and 3, respectively).

After the model was established, the geometry optimization and a following isothermal-isobaric NPT ensemble calculation with 500 ps were conducted to relax the system. Then molecular dynamic simulations were carried out. The simulation temperature was set as 298 K, and the pressure was 1 atm. The canonical NVT ensemble with 1 ns was implemented to determine the energy, radial distribution, density distribution, and other parameters. In order to calculate the interfacial tension, another 2 ns NVT calculation was conducted to minimize the statistical error caused by pressure fluctuations.

3. Results and discussion

3.1 Validation of force field

The adaptability and reliability of the applied COMPASS force field for n-decane and water systems were firstly validated. Fig. 3 presents the density distributions of the water/n-decane system at equilibrium. It is observed that the densities of n-decane and water were close to 746 and 996 $kg \cdot m^{-3}$, which are consistent with the experimental data of 734 and 998 $kg \cdot m^{-3}$ under ambient condition (298 K, 1 atm). It is noteworthy that the densities around the oil-water interface fluctuate, which was also mentioned in the previous work by Wick et al. [51]. It is believed that the fluctuations of the density distributions would not disappear until they are far from the interface. Similarly, this phenomenon was reported in water/n-hexane and water/n-alkane systems [52, 53]. Thus, the determination of interface thickness is of importance for

investigating the characteristics of interface. The commonly applied method to calculate the thickness is the 90–90% principle, in which the distance between 90% of oil density and 90% of water phase density is used as the thickness of the oil-water interface. The interface thickness of the system was calculated as 0.54 nm, which is close to the experimental data of 0.46 ± 0.02 nm [54].

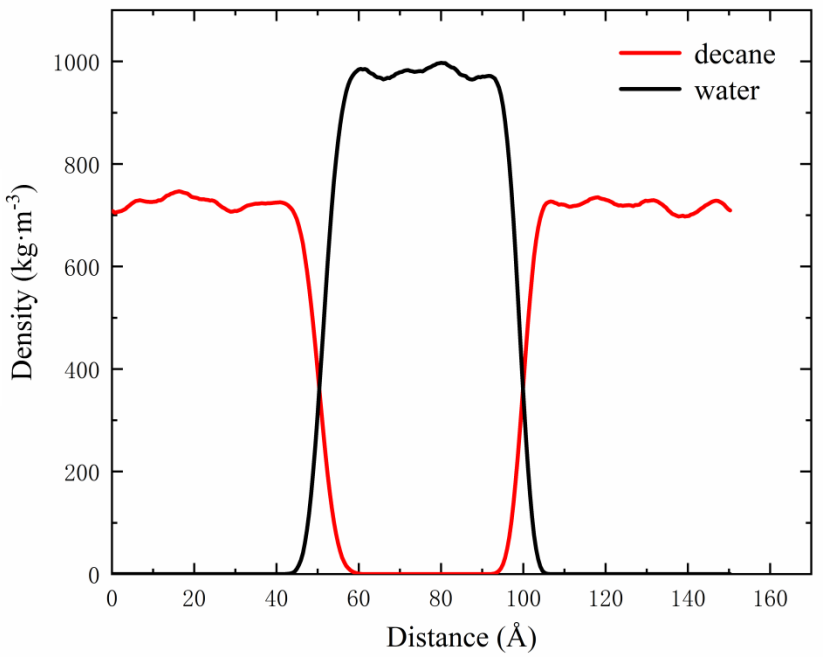

Fig. 3. Density distribution profiles of water/n-decane system.

As is known, the interfacial tension is determined by the pressure in the normal direction and tangential direction at the interface, which can be written as [55]:

$$\gamma = \langle \frac{L_z}{2} \left[P_z - \frac{P_x + P_y}{2} \right] \rangle \quad (4)$$

where P_z denotes the pressure component perpendicular to the interface. P_x and P_y are the pressure components along the tangential directions of the interface, and L_z is the length of simulation box perpendicular to the interface.

Without surfactants, the calculated interfacial tension of pure water/n-decane system was 54.28 mN/m, which is consistent with the experimental data of 52.50 mN/m under ambient condition [54]. Therefore, the employed force field has been justified and can be used to describe the microscale interfacial interactions in oil-water system.

3.2 Interfacial characteristics of pure surfactant at oil-water interface

In this section, the performances of pure surfactant at oil-water interface were focused. Firstly, the morphology of pure DTAC surfactant D60 system at the interface was examined. Fig. 4(a) presents the angle distribution between the surfactant molecule and normal direction of interface, and the molecular morphology of surfactant molecules at the interface is shown in Fig. 4(b). It is found that most of DTAC molecules were perpendicular to the interface and seldom bent. It can be attributed to the strong charge repulsion between head groups of cationic DTAC surfactant. This feature of DTAC surfactant makes it difficult to form a dense layer at the interface. However, it would be favorable for the further diffusion of surfactant molecules to the interface.

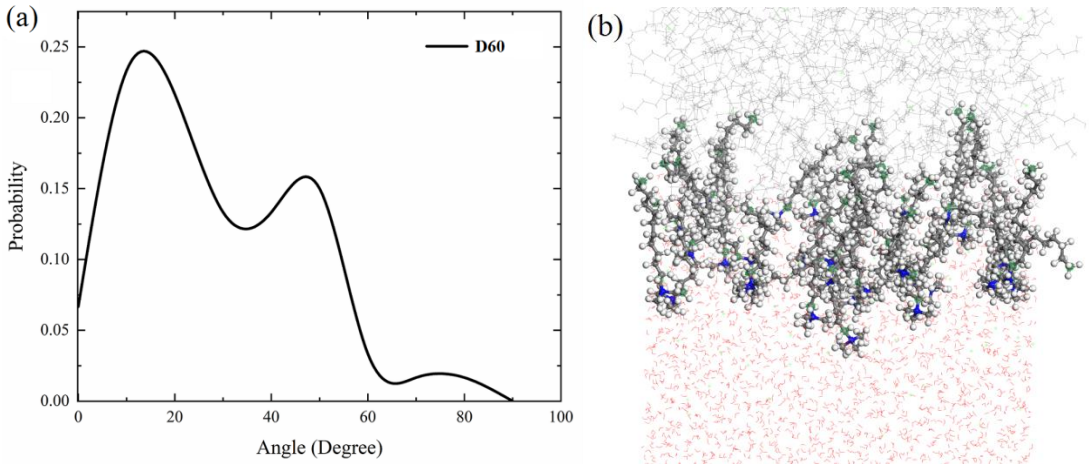

Fig. 4. (a) The angle distribution and (b) molecular morphology of D60 system.

For anionic-nonionic AES surfactant, due to the introduction of non-ionic fragments, the repulsion between head groups was greatly weakened. In this regard, AES surfactants might be more favorable for the formation of adsorption layer at the interface. However, some drawbacks with the interfacial behaviors of AES surfactants have also been observed, which might be unfavorable for the formation of a dense adsorption layer. As illustrated in Fig. 5(a), only a small number of molecules maintained the morphology perpendicular to the interface, most of AES molecules exhibited different degrees of bending, which would hinder the diffusion of surfactant to the interface and also affect the oil displacement efficiency. It should be noted that when pure AES or mixed surfactant systems are considered, the EO number was

chosen as 3. The influences of EO number will be discussed later. To understand the arrangement of surfactants more clearly, the angles θ_1, θ_2 between hydrophobic, hydrophilic groups of AES surfactant $C_{12}EO_3S$ and normal direction of interface, i.e., Z-axis, were defined, as shown in Fig. 5(b). The calculations of θ_1 and θ_2 are as follows:

$$\cos\theta = \frac{|Z_1 - Z_2|}{\sqrt{(X_1-X_2)^2+(Y_1-Y_2)^2+(Z_1-Z_2)^2}} \quad (5)$$

where X_1, Y_1, and Z_1 are the coordinates of C_1 or O_1. X_2, Y_2, and Z_2 are the coordinates of C_{12} or O_4. The value of $(Z_1+Z_2)/2$ is used to represent the centroid of the group.

Fig. 6(a) presents the distributions of inclination angles with the centroids of the hydrophobic and hydrophilic groups of AES $C_{12}EO_3S$ molecules. The probability profiles of inclination angles are presented in Fig. 6(b). It is found the angles θ_1 between hydrophobic groups and Z-axis were mainly in the range of 60–80°, while the angles θ_2 between hydrophilic groups and Z-axis were mostly distributed within 40–70°. It suggests that when pure anionic-nonionic AES surfactant is adopted, the hydrophobic groups tend to lie flatly at the interface, which would result in great steric hindrance for diffusion to the interface.

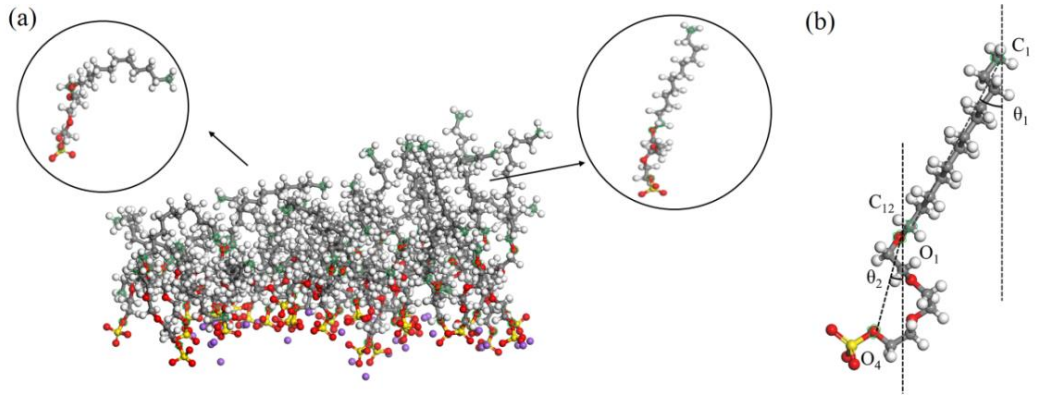

Fig. 5. (a) The molecular morphology of AES molecules at oil-water interface (both oil and water molecules were removed for clarity); (b) definitions of inclination angles θ_1 and θ_2.

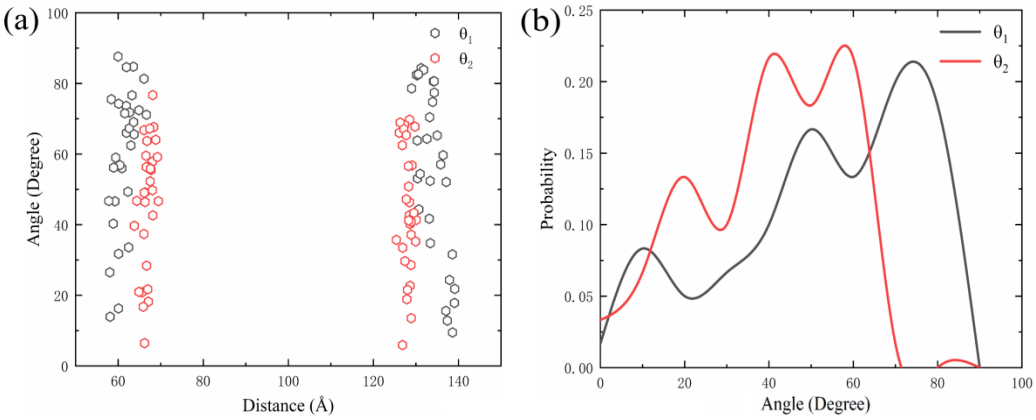

Fig. 6. (a) Distributions of θ_1 and θ_2; (b) probability profiles of θ_1 and θ_2.

3.3 Interfacial characteristics of mixed surfactant system at oil-water interface

Due to the abovementioned limitations of single type of surfactant, the synergy of binary mixture of DTAC and AES surfactants at oil-water interface were investigated in this section. Fig. 7 depicts the radial distribution function (RDF) between the head groups of each system, reflecting the relationship between the local and global distribution of particles. It should be mentioned that pure surfactants AES and DTAC were also examined for comparison. It is observed that when pure DTAC surfactant, i.e., D60 system, was applied, the RDF peak appeared at the distance of 8.75 Å and the peak value was relatively low compared with other mixed and pure AES systems. It indicates that the distribution of pure DTAC surfactant was more dispersed because of strong charge repulsion between head groups. For pure AES surfactant S60 system, the RDF peak appeared much earlier and the peak value increased. With the addition of AES into DTAC surfactant, the mutual attraction between sulfate and quaternary ammonium groups reduced the distance between them. For the S12D48 system, it is found that two peaks were formed. The first peak was formed due to the interactions between the sulfate groups of AES molecules as well as the interactions between sulfate and quaternary ammonium groups. The second peak corresponded to the interactions between the quaternary ammonium groups. With the increase of AES concentration, the value of the second peak also gradually decreased. From the perspective of RDF distribution, the systems of S30D30 and S36D24 were found to have the best interfacial performances. The reason for the S30D30 system was that the

ratio of anion to cation head group was 1:1, which had a good electric balance. Although S36D24 system did not reach the charge balance, the much more non-ionic fragments introduced by C12EO3S molecules reduced the repulsion between head groups, thereby achieving a relatively dense surfactant adsorption layer.

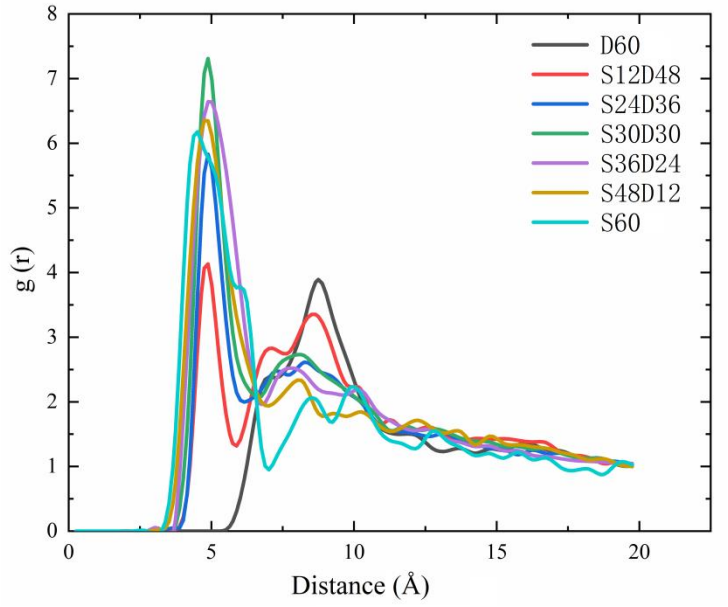

Fig. 7. The RDF profiles between head groups of different surfactant systems.

In addition, the interface formation energy (IFE) of different surfactant systems was studied. The IFE value is related to the interaction forces between surfactant and water/oil molecules:

$$\mathrm{IFE} = \frac{\mathrm{E_{total}} - n\mathrm{E_{surfactant}} - \mathrm{E_{oil/water\ interface}}}{n} \quad (6)$$

where $\mathrm{E_{total}}$ denotes the total energy of the system, and $\mathrm{E_{surfactant}}$ is the energy of single surfactant molecule. $\mathrm{E_{oil/water\ interface}}$ represents the energy of the system without surfactant at oil-water interface, and n is the number of surfactant molecules adsorbed at the interface. For surfactant system, the more negative the IFE value is, the stronger ability the surfactant has to reduce the interfacial tension.

It is observed that the stabilities of the mixed systems were much higher than those of pure cationic surfactants, as displayed in Fig. 8. When pure DTAC surfactant was adopted, the IFE of the system was around –176 kJ·mol^{-1}. With the addition of AES surfactant, the negative charge of sulfate groups would neutralize part of the positive charge of DTAC molecules, which could weaken the repulsion between molecules.

Therefore, the bindings between the molecules became stronger, and the IFE decreased gradually. For pure AES surfactant system, due to the introduction of non-ionic fragments, the anionic characteristics of surfactant were weakened, and therefore the head groups were arranged more tightly. Compared with pure DTAC system, the IFE of AES system exhibited an obvious improvement. It is found that S30D30 and S36D24 exhibited superior performances comparing with other mixed and pure surfactants, which is consistent with the analyses by RDF distributions.

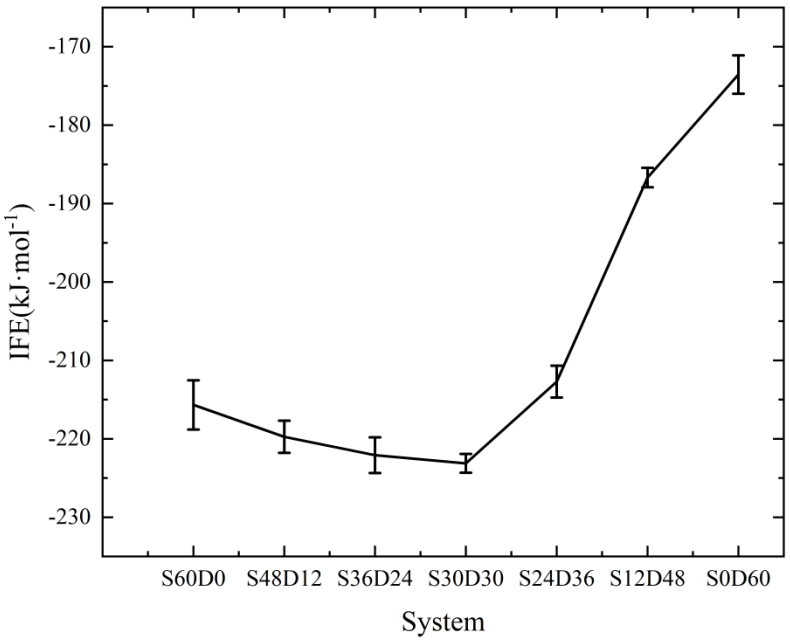

Fig. 8. The IFE values of different mixed surfactant systems.

As discussed before, the main issue of pure AES system lies in the horizontal arrangement of surfactant carbon chains, which makes it difficult to form a dense surfactant layer. As for DTAC molecules, the hydrophobic groups tend to be arranged vertically at oil-water interface. By adding AES into DTAC system, the sulfate group of $C_{12}EO_3S$ molecules had an attractive effect on DTAC molecules. Thus, DTAC molecules could attract AES molecules to achieve better interfacial performances. Fig. 9(a) displays the distribution of hydrophobic group angle of $C_{12}EO_3S$ molecules θ_1 in S60 and S30D30 systems. It is found that with the addition of AES, the interfacial behavior of the mixed system was greatly improved. The peak value was reduced from 70–80° to 30–40°, indicating that the hydrophobic groups became more

perpendicular to the interface and penetrated the oil phase to interact with oil. Compared with pure AES molecular configurations shown in Fig. 5(a), the improvement of the interfacial behavior of mixed system could also be obviously observed in Fig. 9(b). Fig. 10 presents the top views of surfactant layers. It can be seen that due to the better interfacial behaviors of mixed system and smaller volume of DTAC molecules compared with AES molecules, it could free up much more space to absorb more surfactant molecules at the interface, thus increasing the critical micelle concentration (CMC) of surfactant.

Finally, continuous 2 ns NVT simulations were performed for S60, S30D30 and D60 surfactant systems. Each system was calculated three times to determine the interfacial tension. The calculated interfacial tensions for S60, S30D30 and D60 systems were 20.01±0.46, 17.41±1.78, and 23.71±1.11 mN/m, respectively. These results were basically in line with the above discussions. It is found that the interfacial tension of mixed surfactant system S30D30 was decreased compared with pure AES and DTAC surfactant, with more obvious improvement than DTAC. Compared with AES surfactant, S30D30 only exhibited a slight improvement. However, the mixed surfactant system shows more advantageous performances than AES on salt resistance, which will be discussed later.

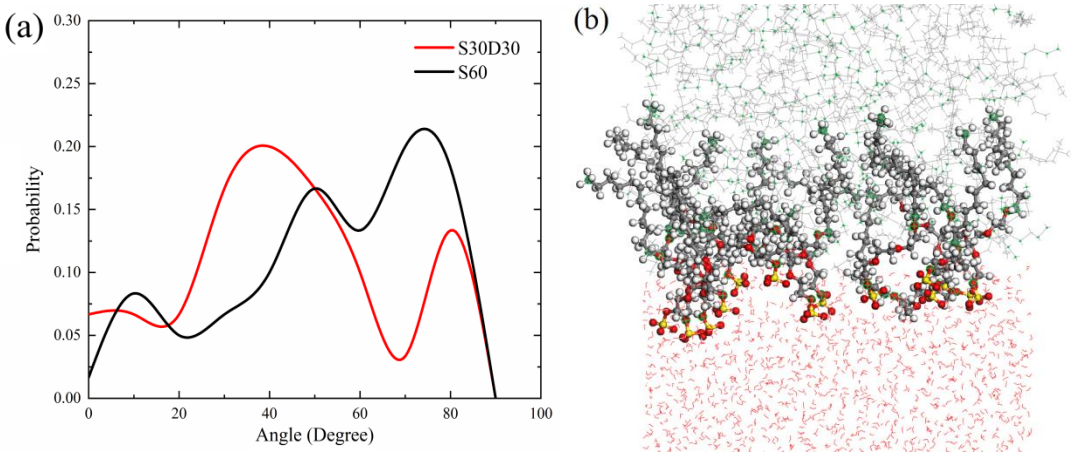

Fig. 9. (a) Distribution of θ_1 in S60 and S30D30 systems; (b) molecular morphology of AES $C_{12}EO_3S$ molecules at oil-water interface in S30D30 system (DTAC molecules were removed for clarity).

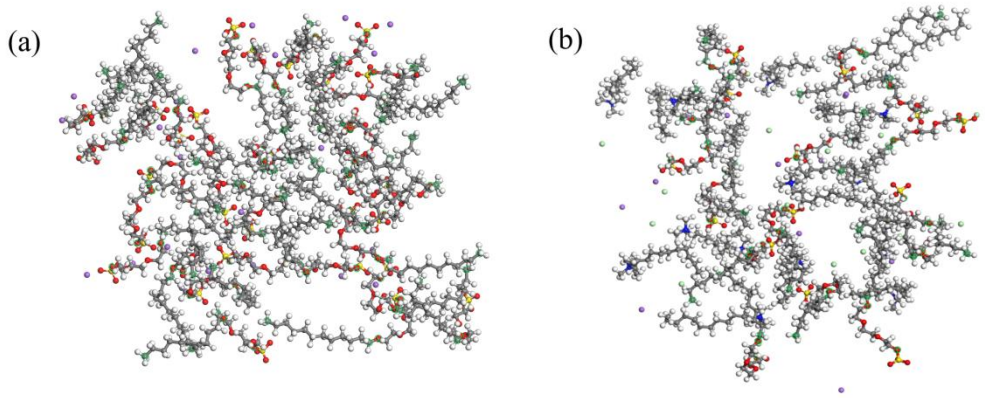

Fig. 10. Top view of the surfactant layer in (a) S60 system; (b) S30D30 system.

3.4 Effect of EO number on mixed surfactant system

In order to investigate the influence of EO group of AES molecules on the performances of mixed surfactants, three systems, i.e., EO3, EO5, and EO7, were established corresponding to the EO group number of 3, 5, and 7, respectively. The interface formation energy IFE was firstly calculated, as shown in Table 2. It is found that with the increase of EO group number, the IFE gradually decreased from –222.39 to –179.33 kJ·mol^{-1}, and therefore the stability of interface became worse. It should be noted that the mixing ratio was fixed as 5:5 when the effects of EO number were concerned.

Table 2. Total energy and IFE of mixed systems with different EO group numbers.

System	E_{AES} (kJ·mol^{-1})	E_{ref} (kJ·mol^{-1})	E_{DTAC} (kJ·mol^{-1})	E_{total} (kJ·mol^{-1})	IFE (kJ·mol^{-1})
EO3	-952.90	-141265.87	-146.37	-187587.79	-222.39
EO5	-965.35	-141265.87	-146.37	-186703.93	-201.44
EO7	-978.58	-141265.87	-146.37	-185774.23	-179.33

To reveal the underlying mechanism, the RDF profiles of surfactants with different EO group numbers were studied, as presented in Fig. 11. It is observed that the trends of the systems with different EO group numbers were similar. However, for the EO3 system, the peak value was as high as 6.74, which was larger than that of EO5 and EO7 systems. This is due to that the further introduction of EO group of AES molecules would increase the steric hindrance, which is not conducive to the

formation of a dense surfactant layer.

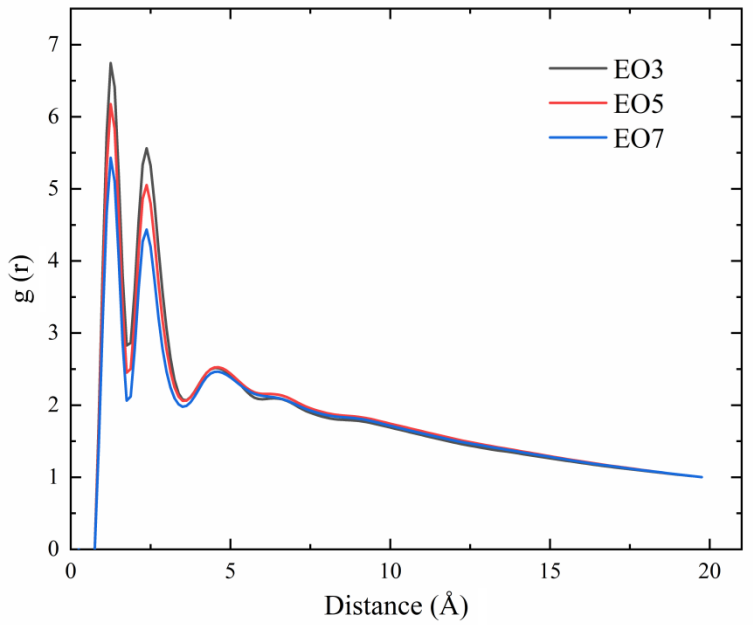

Fig. 11. The RDF profiles between surfactants with different EO group numbers.

In order to understand the structures of surfactant molecules at the interface more intuitively, the distributions of the angles between the hydrophobic and hydrophilic groups of AES molecules and Z-axis in each system were examined. With the increment of EO group number, the length of hydrophilic group of AES molecule increase. Thus, the angles between the hydrophilic group and Z-axis should be re-defined, as illustrated in Fig. 12. The distributions of the hydrophobic group angles θ_1 and hydrophilic group angles θ_2 in different systems are displayed in Fig. 13. From the figure, it is observed that with the increase of EO group number, the surfactant molecules exhibited different degrees of bending. In EO3 system, the angle of hydrophobic group was mostly distributed within the range of 30–50°, while the angle of hydrophilic group was within 10–50°. In EO5 system, the angle of hydrophobic groups was within 40–70°, but hydrophilic group had larger degree of bending of 60–90°. This indicates that in EO5 system, the hydrophilic groups were basically in horizontal state, which would prevent the formation of a dense surfactant layer. As for EO7 system, it is found that hydrophilic groups exhibited better interfacial behaviors. However, the distribution of hydrophobic groups became worse with most of them

distributed in 70–90°. Therefore, it can be concluded that the increase of EO group number would cause the surfactants to bend with different degrees, which could create steric hindrance and reduce the tightness of surfactants' arrangement at the interface.

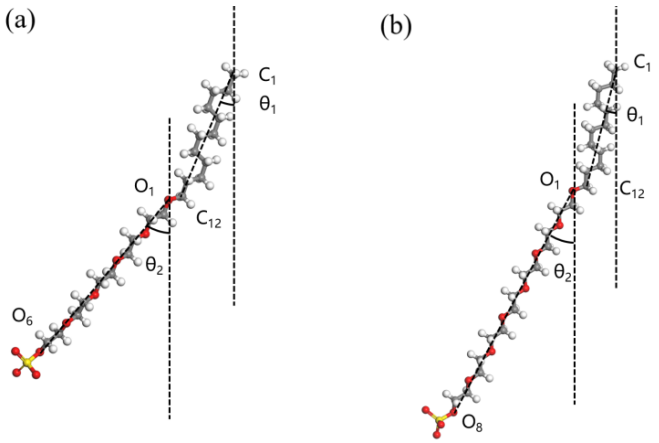

Fig. 12. The definitions of θ_1 and θ_2 of (a) $C_{12}EO_5S$; (b) $C_{12}EO_7S$ molecule.

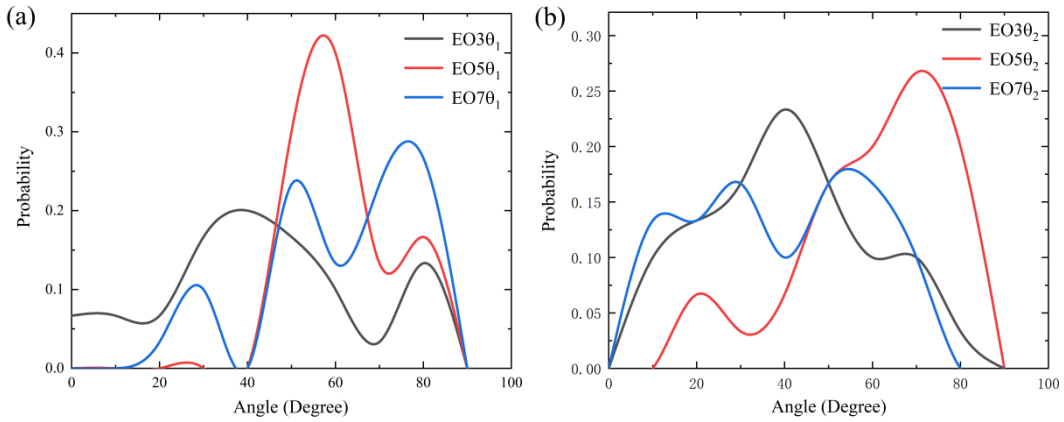

Fig. 13. The angle distributions of (a) hydrophobic and (b) hydrophilic groups of AES molecules in mixed systems with different EO group numbers.

3.5. Salt resistance of mixed surfactant system

As is known, the actual situation of oil reservoirs is usually under harsh conditions of high salinity and high temperature. Thus, the salt tolerance of the applied surfactant system is of great significance. The effect of saltwater on the surfactant is mainly reflected by the interactions between salt ions, e.g., Ca^{2+}, Mg^{2+}, surfactants and water molecules. Salt ions could attract the oxygen atoms of water molecules, thereby reducing the number of water molecules near the head group of surfactants, which would destroy the structure of hydration shell and deteriorate the function of

surfactants.

To investigate the impacts of salt environment on the surfactants, 20 Ca^{2+} and 40 Cl^{-} (3.37 wt%) were randomly added to the water phase of three systems, i.e., S60, S30D30, and D60. The snapshots of Ca^{2+} ions movement are displayed in Fig. 14. It should be mentioned that the simulation case was run for 1.5 ns with the migration of salt ions more obvious in the first stage of 500 ps. The salt ions then gradually tended to be in equilibrium. Thus, the stage of first 500 ps was focused to analyze the migration of salt ions. It is found that most of Ca^{2+} ions were in water phase at the beginning with only a small part locating near the head groups of surfactants. With time going on, Ca^{2+} ions were attracted by the sulfate groups and gradually accumulated near AES surfactants due to their negative charge properties, resulting in poor salt resistance, as shown in Fig. 14(a). As for cationic DTAC surfactant, it exhibited repelling effect on salt ions and the accumulation of salt ions near DTAC surfactants could be avoided due to the positive charge on the head groups, as shown in Fig. 14(c). It can be observed that at the time of 500 ps, there was almost no Ca^{2+} ion near the head groups of DTAC surfactants, reflecting the strong salt resistance of cationic surfactants. Fig. 14(b) shows the snapshots of Ca^{2+} ions in the mixed system. It is observed the salt resistance of the mixed system was obviously superior to pure AES surfactant but inferior to pure DTAC surfactant.

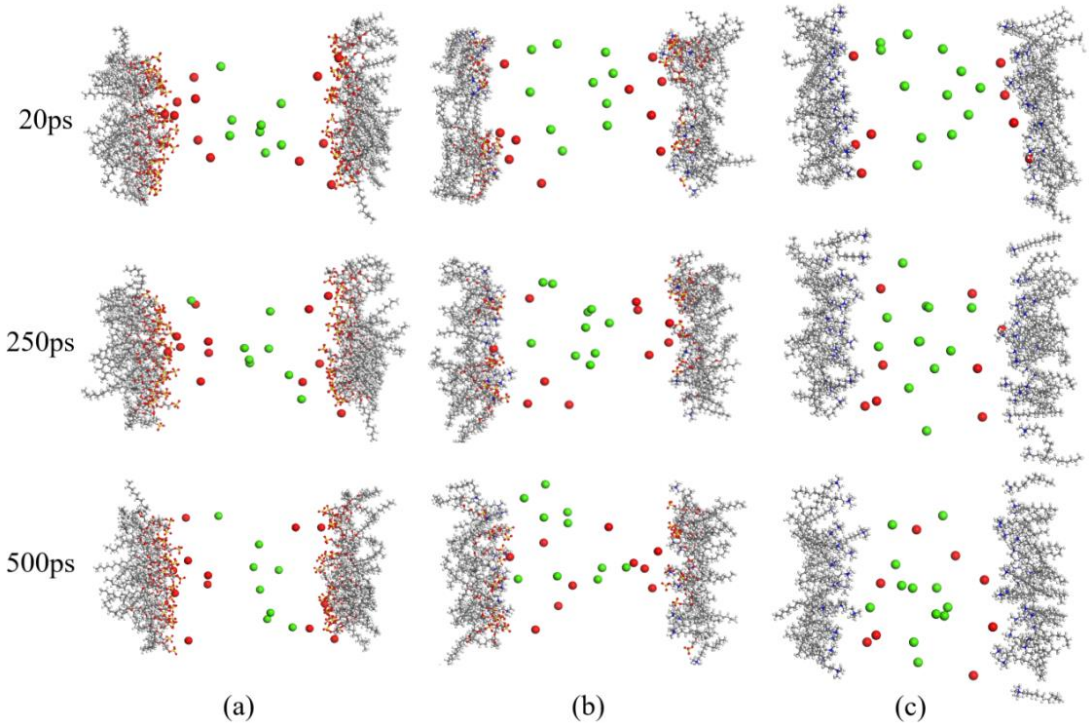

Fig. 14. The snapshots of Ca^{2+} ions movement in different systems: (a) S60; (b) S30D30; (c) D60 (red and green spheres represent the Ca^{2+} ions near and apart from the head groups of surfactants, respectively; water, oil molecules and Cl^- ions were removed for clarity).

To specifically describe the performances of salt resistance, the density distribution profiles of Ca^{2+} ions of each system were calculated to analyze their movement tendency, as presented in Fig. 15. It should be mentioned that the density distribution profiles were determined by the average over a time period of 100 ps. The migration of salt ions can be clearly observed through the density peak and the position of the peak. For pure AES S60 system, at the first stage of 0–100 ps, the distribution of Ca^{2+} ions was mainly concentrated around 91.5 Å and 113.36 Å, which was located in water phase. With time passing by, the peak value of Ca^{2+} ions in water phase decreased, while the peak value near the surfactant gradually increased. In the later stage of simulation, the positions of peaks moved to 72.77 Å and 118.31 Å with the peak values of 19.03 and 19.01, respectively. It indicates that Ca^{2+} ions aggregated near the head groups of AES molecules. For S30D30 system, it is found that Ca^{2+} ions accumulated at oil-water interface forming two peaks at the first stage. With time

going on, the peak value gradually decreased and moved to the water phase, which implies that the salt resistance of mixed surfactant system was improved by adding DTAC surfactant. The same trend was observed in D60 system. The peak of Ca^{2+} ions clearly moved to water phase and the densities of Ca^{2+} ions near the interface greatly decreased or even disappeared. The positions where Ca^{2+} ions first appeared had a clear tendency to move to water phase from the interface with the time passing by, indicating the strong repulsion of cationic surfactant to salt ions.

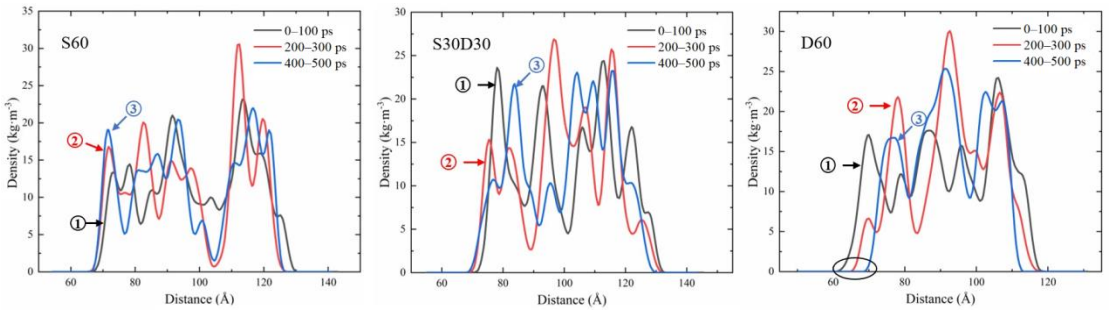

Fig. 15. Density distribution profiles of Ca^{2+} ions at different times in different surfactant systems.

Furthermore, the RDF profiles between Ca^{2+} ions and the head groups of surfactants were examined to investigate the aggregation level of salt ions. It is observed from Fig. 16 that for cationic surfactant DTAC, there was not density peak formed near the head group. In addition, the concentration of Ca^{2+} ions near the head group was far less than that in water phase, indicating strong salt resistance of DTAC surfactant. For S60 and S30D30 systems, the distribution trends of Ca^{2+} ions were similar. However, due to the introduction of cationic surfactants in S30D30 system, the concentration of Ca^{2+} ions near the sulfate group in the mixed system decreased obviously. The first peak decreased from 3.11 to 2.29, and the second peak decreased from 1.87 to 0.91. It suggests that compared with anionic-nonionic surfactant, the introduction of cationic surfactants could improve the overall salt resistance of mixed surfactant system. In realistic applications, the mixing ratio and other properties of mixed surfactant systems should be determined by the actual conditions of reservoir pore structure, salinity, etc.

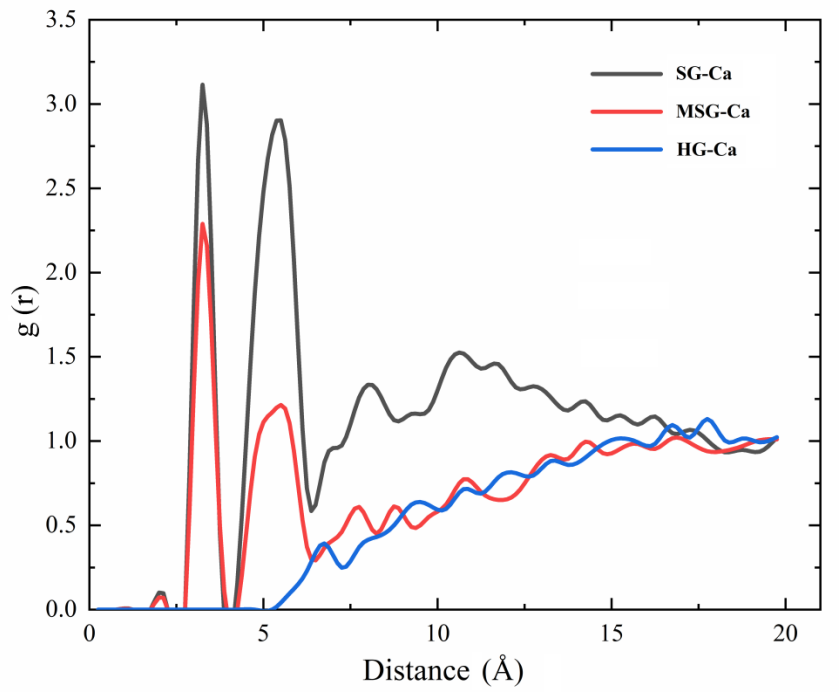

Fig. 16. The RDF profiles between surfactant head groups and Ca^{2+} ions (SG, MSG and HG refer to the sulfate group in S60, sulfate group in S30D30 and hydrophilic group in D60 system, respectively).

4. Conclusions

In this work, molecular dynamics simulations were employed to investigate the interfacial properties and molecular behaviors at the microscopic level of pure anionic-nonionic and cationic surfactant as well as their mixtures at oil-water interface. The following conclusions have been drawn:

(1) When pure cationic surfactant DTAC was applied, there was a great repulsion between surfactant molecules due to the positive charges of head groups, which is unfavorable for forming a dense surfactant layer. However, most of DTAC molecules were found perpendicular to the interface, indicating excellent interfacial behavior for further diffusion of surfactant molecules to the interface. For pure anionic-nonionic surfactant AES, the addition of non-ionic fragments has weakened the repulsion between head groups. However, most of hydrophobic groups of surfactant molecules were found bent at the interface, which would lead to steric hindrance on the further diffusion of surfactant molecules.

(2) By mixing AES and DTAC surfactants, the sulfate group of AES could attract

DTAC molecules, thereby reducing the repulsion between head groups and forming a dense surfactant adsorption layer. Meanwhile, as DTAC molecules existed near AES molecules, the interactions between head groups could improve the interfacial behavior of AES molecules.

(3) With the increase of EO group number of AES molecule, the surfactant molecules could be bent at different degrees, which would hinder the further diffusion of surfactants. By introducing an appropriate number of EO group, not only the precipitation could be avoided, but also the improved interfacial behaviors could be achieved.

(4) The cationic surfactant presents obvious superior performance on salt resistance than anionic-nonionic surfactant. The addition of cationic surfactant DTAC into anionic-nonionic surfactant AES could enhance the overall performance of salt resistance of the mixed surfactants. The mixed system of anionic-nonionic surfactant AES and cationic surfactant DTAC with the ratio 1:1, i.e., S30D30 system, shows the optimal overall performances on interfacial behaviors and salt resistance.

Acknowledgements

This work was supported by the National Natural Science Foundation of China (Grant Nos. 51706018, 52076012) and the Fundamental Research Funds for the Central Universities (Grant Nos. FRF-TP-19-009A3, FRF-BD-20-09A).

References

[1] Y. Duan, J. Feng, Y. Zhu, H. Li, X. Liu, H. Zhou, W. Li, A systematic approach to measure the contents of mono- and di-sulfonates in petroleum sulfonates by the novel method of acid–base titration coupled with traditional two-phase titration, RSC Adv., 8(67) (2018) 38606-38613.

[2] A. Agi, R. Junin, M.O. Abdullah, M.Z. Jaafar, A. Arsad, W.R. Wan Sulaiman, M.N.A.M. Norddin, M. Abdurrahman, A. Abbas, A. Gbadamosi, N.B. Azli, Application of polymeric nanofluid in enhancing oil recovery at reservoir condition, J. Petrol. Sci. Eng., 194 (2020) 107476.

[3] K.R. Chaturvedi, T. Sharma, Carbonated polymeric nanofluids for enhanced oil recovery from sandstone reservoir, J. Petrol. Sci. Eng., 194 (2020) 107499.

[4] N.K. Jha, A. Ivanova, M. Lebedev, A. Barifcani, A. Cheremisin, S. Iglauer, J.S. Sangwai, M. Sarmadivaleh, Interaction of low salinity surfactant nanofluids with carbonate surfaces and molecular level dynamics at fluid-fluid interface at ScCO2 loading, J. Colloid Interface Sci., 586 (2021) 315-325.

[5] R. Singh, K.K. Mohanty, Synergy between Nanoparticles and Surfactants in Stabilizing Foams for Oil Recovery, Energy Fuels, 29(2) (2015) 467-479.
[6] W. Yang, T. Wang, Z. Fan, Q. Miao, Z. Deng, Y. Zhu, Foams Stabilized by In Situ-Modified Nanoparticles and Anionic Surfactants for Enhanced Oil Recovery, Energy Fuels, 31(5) (2017) 4721-4730.
[7] A.K. Yegya Raman, C.P. Aichele, Demulsification of Surfactant-Stabilized Water-in-Oil (Cyclohexane) Emulsions using Silica Nanoparticles, Energy Fuels, 32(8) (2018) 8121-8130.
[8] Y. Zhou, X. Wu, X. Zhong, W. Sun, H. Pu, J.X. Zhao, Surfactant-Augmented Functional Silica Nanoparticle Based Nanofluid for Enhanced Oil Recovery at High Temperature and Salinity, ACS Appl. Mater. Interfaces, 11(49) (2019) 45763-45775.
[9] X. Li, Q. Xue, L. Zhu, Y. Jin, T. Wu, Q. Guo, H. Zheng, S. Lu, How to select an optimal surfactant molecule to speed up the oil-detachment from solid surface: A computational simulation, Chem. Eng. Sci., 147 (2016) 47-53.
[10] N. Pal, M. Vajpayee, A. Mandal, Cationic/Nonionic Mixed Surfactants as Enhanced Oil Recovery Fluids: Influence of Mixed Micellization and Polymer Association on Interfacial, Rheological, and Rock-Wetting Characteristics, Energy Fuels, 33(7) (2019) 6048-6059.
[11] H. Zhao, Y. Bai, H. Sun, Y. Li, Study of the molecular array behaviours and interfacial activities of green surfactant alkyl polyglycoside and the mixed systems with other surfactants on oil–water interface, Mol. Simul., 43(13-16) (2017) 1107-1115.
[12] J. Zhou, P.G. Ranjith, Self-assembly and viscosity changes of binary surfactant solutions: A molecular dynamics study, J. Colloid Interface Sci., 585 (2021) 250-257.
[13] R. Saha, R.V.S. Uppaluri, P. Tiwari, Impact of Natural Surfactant (Reetha), Polymer (Xanthan Gum), and Silica Nanoparticles To Enhance Heavy Crude Oil Recovery, Energy Fuels, 33(5) (2019) 4225-4236.
[14] H. Vatanparast, M. Eftekhari, A. Javadi, R. Miller, A. Bahramian, Influence of hydrophilic silica nanoparticles on the adsorption layer properties of non-ionic surfactants at water/heptane interface, J. Colloid Interface Sci., 545 (2019) 242-250.
[15] S. Adkins, P.J. Liyanage, G.W.P. Pinnawala Arachchilage, T. Mudiyanselage, U. Weerasooriya, G.A. Pope, A New Process for Manufacturing and Stabilizing High-Performance EOR Surfactants at Low Cost for High-Temperature, High-Salinity Oil Reservoirs, in: SPE Improved Oil Recovery Symposium, 2010.
[16] L. Torres, A. Moctezuma, J. Avendaño-Gómez, A. Muñoz, J. Gracida-Rodríguez, Comparison of bio- and synthetic surfactants for EOR, J. Petrol. Sci. Eng., 76 (2011) 6-11.
[17] H. Wang, Z. Qu, Y. Yin, J. Bai, B. Yu, Review of Molecular Simulation Method for Gas Adsorption/desorption and Diffusion in Shale Matrix, J. Therm. Sci., 28(1) (2019) 1-16.
[18] W. Zhou, H. Wang, X. Yang, X. Liu, Y. Yan, Confinement Effects and CO2/CH4 Competitive Adsorption in Realistic Shale Kerogen Nanopores, Ind. Eng. Chem. Res., 59(14) (2020) 6696-6706.
[19] W. Zhou, H. Wang, Y. Yan, X. Liu, Adsorption Mechanism of CO2/CH4 in Kaolinite Clay: Insight from Molecular Simulation, Energy Fuels, 33 (2019) 6542-6551.
[20] C. Chen, W. Hu, L. Yang, J. Zhao, Y. Song, Gas supersaturation and diffusion joint controlled CH4 nanobubble evolution during hydrate dissociation, J. Mol. Liq., 323 (2021) 114614.
[21] T.A. Ho, L.J. Criscenti, Molecular-level understanding of gibbsite particle aggregation in water, J. Colloid Interface Sci., 600 (2021) 310-317.
[22] T. Wu, Q. Xue, X. Li, Y. Tao, Y. Jin, C. Ling, S. Lu, Extraction of kerogen from oil shale with

supercritical carbon dioxide: Molecular dynamics simulations, J. Supercrit. Fluids, 107 (2016) 499-506.
[23] W. Zhou, H. Wang, Z. Zhang, H. Chen, X. Liu, Molecular simulation of CO2/CH4/H2O competitive adsorption and diffusion in brown coal, RSC Adv., 9(6) (2019) 3004-3011.
[24] X. Tang, S. Xiao, Q. Lei, L. Yuan, B. Peng, L. He, J. Luo, Y. Pei, Molecular Dynamics Simulation of Surfactant Flooding Driven Oil-Detachment in Nano-Silica Channels, J. Phys. Chem. B, 123(1) (2019) 277-288.
[25] X. Sun, H. Zeng, T. Tang, Effect of non-ionic surfactants on the adsorption of polycyclic aromatic compounds at water/oil interface: A molecular simulation study, J. Colloid Interface Sci., 586 (2021) 766-777.
[26] F.T. Varel, C. Dai, A. Shaikh, J. Li, N. Sun, N. Yang, G. Zhao, Chromatography and oil displacement mechanism of a dispersed particle gel strengthened Alkali/Surfactant/Polymer combination flooding system for enhanced oil recovery, Colloid Surface A, 610 (2021) 125642.
[27] E. Riccardi, T. Tichelkamp, Calcium ion effects on the water/oil interface in the presence of anionic surfactants, Colloid Surface A, 573 (2019) 246-254.
[28] H. Jia, P. Lian, H. Yan, Y. Han, Q. Wang, J. Dai, S. Wang, Z. Tian, D. Wang, Insights into the Assembly of the Pseudogemini Surfactant at the Oil/Water Interface: A Molecular Simulation Study, Langmuir, 36(7) (2020) 1839-1847.
[29] P. Shi, H. Zhang, L. Lin, C. Song, Q. Chen, Z. Li, Molecular dynamics simulation of four typical surfactants at oil/water interface, J. Dispersion Sci. Technol., 39(9) (2017) 1258-1265.
[30] A.A. Ivanova, A.N. Cheremisin, A. Barifcani, S. Iglauer, C. Phan, Molecular insights in the temperature effect on adsorption of cationic surfactants at liquid/liquid interfaces, J. Mol. Liq., 299 (2020) 112104.
[31] H. Yan, S.L. Yuan, G.Y. Xu, C.B. Liu, Effect of Ca2+ and Mg2+ ions on surfactant solutions investigated by molecular dynamics simulation, Langmuir, 26(13) (2010) 10448-10459.
[32] H. Jia, P. Lian, X. Leng, Y. Han, Q. Wang, K. Jia, X. Niu, M. Guo, H. Yan, K. Lv, Mechanism studies on the application of the mixed cationic/anionic surfactant systems to enhance oil recovery, Fuel, 258 (2019) 116156.
[33] Z. Li, H. Wu, Y. Hu, X. Chen, Y. Yuan, Y. Luo, J. Hou, B. Bai, W. Kang, Ultra-low interfacial tension biobased and catanionic surfactants for low permeability reservoirs, J. Mol. Liq., 309 (2020) 113099.
[34] X. Liu, Y. Zhao, Q. Li, T. Jiao, J. Niu, Adsorption behavior, spreading and thermal stability of anionic-nonionic surfactants with different ionic headgroup, J. Mol. Liq., 219 (2016) 1100-1106.
[35] Z.-Y. Liu, Z.-Q. Li, X.-W. Song, J.-C. Zhang, L. Zhang, L. Zhang, S. Zhao, Dynamic interfacial tensions of binary nonionic–anionic and nonionic surfactant mixtures at water–alkane interfaces, Fuel, 135 (2014) 91-98.
[36] Q. Zhang, Y. Li, Y. Song, H. Fu, J. Li, Z. Wang, Properties of vesicles formation of single-chain branched carboxylate anionic surfactant in aqueous solutions, J. Mol. Liq., 243 (2017) 431-438.
[37] B. Hu, Effect of Cationic and Zwitterionic Surfactants on Contact Angle of Quartz–Water–Crude Oil System, J. Dispersion Sci. Technol., 37(11) (2015) 1555-1562.
[38] W. Qiao, Y. Cui, Y. Zhu, H. Cai, Dynamic interfacial tension behaviors between Guerbet betaine surfactants solution and Daqing crude oil, Fuel, 102 (2012) 746-750.
[39] B. Song, X. Hu, X. Shui, Z. Cui, Z. Wang, A new type of renewable surfactants for enhanced oil recovery: Dialkylpolyoxyethylene ether methyl carboxyl betaines, Colloid Surface A, 489 (2016)

433-440.
[40] L. Zhou, H. Chen, X. Jiang, F. Lu, Y. Zhou, W. Yin, X. Ji, Modification of montmorillonite surfaces using a novel class of cationic gemini surfactants, J. Colloid Interface Sci., 332(1) (2009) 16-21.
[41] B. Gao, M.M. Sharma, A family of alkyl sulfate gemini surfactants. 2. Water–oil interfacial tension reduction, J. Colloid Interface Sci., 407 (2013) 375-381.
[42] O. Massarweh, A.S. Abushaikha, The use of surfactants in enhanced oil recovery: A review of recent advances, Energy Rep., 6 (2020) 3150-3178.
[43] M.S. Kamal, A Review of Gemini Surfactants: Potential Application in Enhanced Oil Recovery, J. Surfactants Deterg., 19(2) (2016) 223-236.
[44] H.-Y. Cai, Y. Zhang, Z.-Y. Liu, J.-G. Li, Q.-T. Gong, Q. Liao, L. Zhang, S. Zhao, Molecular dynamics simulation of binary betaine and anionic surfactant mixtures at decane - Water interface, J. Mol. Liq., 266 (2018) 82-89.
[45] H. Feng, J. Hou, T. Ma, Z. Meng, H. Wu, H. Yang, W. Kang, The ultra-low interfacial tension behavior of the combined cationic/anionic-nonionic gemini surfactants system for chemical flooding, Colloid Surface A, 554 (2018) 74-80.
[46] Q. Zhang, Y. Li, Y. Song, J. Li, Z. Wang, Adsorption behavior of branched polyoxyethylene ether carboxylate surfactants, Colloid Surface A, 538 (2018) 361-370.
[47] Q.-L. Zhong, X.-L. Cao, Y.-W. Zhu, B.-D. Ma, Z.-C. Xu, L. Zhang, G.-Y. Ma, L. Zhang, Studies on interfacial tensions of betaine and anionic-nonionic surfactant mixed solutions, J. Mol. Liq., 311 (2020) 113262.
[48] S.-S. Sheng, X.-L. Cao, Y.-W. Zhu, Z.-Q. Jin, L. Zhang, Y. Zhu, L. Zhang, Structure-activity relationship of anionic-nonionic surfactant for reducing interfacial tension of crude oil, J. Mol. Liq., 313 (2020) 112772.
[49] T. Ma, H. Feng, H. Wu, Z. Li, J. Jiang, D. Xu, Z. Meng, W. Kang, Property evaluation of synthesized anionic-nonionic gemini surfactants for chemical enhanced oil recovery, Colloid Surface A, 581 (2019) 123800.
[50] H. Sun, COMPASS: An ab Initio Force-Field Optimized for Condensed-Phase ApplicationssOverview with Details on Alkane and Benzene Compounds, J. Phys. Chem. B, 102 (1998) 7338-7364.
[51] C.D. Wick, T.-M. Chang, J.A. Slocum, O.T. Cummings, Computational Investigation of the n-Alkane/Water Interface with Many-Body Potentials: The Effect of Chain Length and Ion Distributions, J. Phys. Chem. C, 116(1) (2012) 783-790.
[52] Y. Aray, J.G. Parra, D.M. Jiménez, R. Paredes, A. Martiz, S. Samaniego, M. Cornejo, E.V. Ludena, C. Paredes, F.J.J.o.C.M.i.S. Ruette, Engineering, Exploring the effect of the O-(1-heptylnonyl) benzene sulfonate surfactant on the nature of the linear hydrocarbons/water interface by means of an atomistic molecular dynamics simulation, J. Comput. Methods Sci. Eng., 17(1) (2017) 39-53.
[53] Huabing, Wang, Carlson, Eric, Henderson, Douglas, Rowley, Richard, L.J.M. Simulation, Molecular Dynamics Simulation of the Liquid-liquid Interface for Immiscible and Partially Miscible Mixtures, Mol. Simul., 29(12) (2003) 777-785.
[54] D.M. Mitrinović, A.M. Tikhonov, M. Li, Z. Huang, S.L. Mark, Noncapillary-Wave Structure at the Water-Alkane Interface, Phys. Rev. Lett., 85(3) (2000) 582-585.
[55] W. Li, Y. Nan, Q. You, Q. Xie, Z. Jin, Effects of salts and silica nanoparticles on oil-brine interfacial properties under hydrocarbon reservoir conditions: A molecular dynamics simulation

study, J. Mol. Liq., 305 (2020) 112860.